The Astrophysical Journal, 804:110 (10pp), 2015 May 10 doi:10.1088/0004-637X/804/2/110

THE CHEMICAL EVOLUTION OF VERY METAL-POOR DAMPED LYα SYSTEMS

David Webster[1], Joss Bland-Hawthorn[2], and Ralph S. Sutherland[3]
[1] Sydney Institute for Astronomy, School of Physics, University of Sydney, NSW 2006, Australia; d.webster@physics.usyd.edu.au
[2] Sydney Institute for Astronomy, School of Physics, University of Sydney, NSW 2006, Australia
[3] Research School of Astronomy & Astrophysics, Australian National University, Cotter Rd, Weston, ACT 2611, Australia
Received 2015 January 7; accepted 2015 April 8; published 2015 May 7

ABSTRACT

In earlier work we showed that a dark matter halo with a virial mass of $10^7\,M_\odot$ can survive feedback from its own massive stars and form stars for $\gtrsim$100 Myr. We also found that our modeled systems were consistent with observations of ultrafaint dwarfs (UFDs), the least massive known galaxies. Very metal-poor damped Lyα systems (DLAs) recently identified at $z \sim 2$ may represent the gas that formed at least some of the observed stars in UFDs. We compare projected sightlines from our simulations to the observed metal-poor DLAs and find that our models can reach the densities of the observed sightlines; however the metallicities are inconsistent with the single supernova simulations, suggesting enrichment by multiple supernovae. We model two scenarios for the history of these systems. The first explains the gas abundances in DLAs by a single burst of star formation. This model can produce the observed DLA abundances, but does not provide an explanation as to why the DLAs show suppressed [α/Fe] compared to the stellar population of UFDs. The second scenario splits the DLAs into a population which is enriched by a single burst, and a population that is enriched by a second burst after the accretion of metal-poor gas. In this scenario, the suppressed average [α/Fe] in DLAs compared to UFDs results from enrichment of second-burst systems by Type Ia supernovae.

Key words: dark ages, reionization, first stars – galaxies: abundances – galaxies: dwarf – galaxies: formation – quasars: absorption lines – stars: Population II

1. INTRODUCTION

The very metal-poor damped Lyα systems (DLAs) with [Fe/H] < -2 recently discovered by Cooke et al. (2011a, 2011b, 2013, 2014) have chemical signatures suggesting that they have experienced only a few enrichment events, making them promising candidates for probing the chemical signatures of the first generations of stars. DLAs absorb light from a bright background source, allowing the detection of gas that is too faint to observe in emission. The most distant and metal-poor DLAs may be the environments of the formation of some of the first generations of stars in the universe. Along with cosmological hydrodynamical simulations (Pontzen et al. 2008; Fumagalli et al. 2011; Cen 2012; Bird et al. 2013), the few DLAs at $z > 2$ that have been detected in emission (Krogager et al. 2012; Jorgenson & Wolfe 2014) suggest that the host galaxies of higher metallicity ($Z \sim 1/50$) DLAs are mostly 10^9–$10^{11}\,M_\odot$ dwarf galaxies.

Cooke et al. (2014) found that the kinematics of the very metal-poor DLAs agreed with those of Milky Way dwarf spheroidal galaxies. Furthermore, the decline in [α/Fe] for [Fe/H] $\gtrsim -2.0$, which is usually assumed to indicate enrichment from Type Ia supernovae (SNe Ia) (Tinsley 1979), is similar to that observed in the dwarf spheroidals, indicative of a similar star formation history. This differs from the Milky Way halo, which shows approximately constant [α/Fe] for $-3.75 <$ [Fe/H] < -0.75. Cooke et al. (2014) therefore suggest that the very metal-poor DLAs correspond to the least massive systems that can form stars at $z \sim 3$.

Over the past decade, a number of galaxies with luminosities below $10^5\,L_\odot$ have been discovered in the local universe. Known as ultrafaint dwarfs (UFDs), these systems are promising candidates for probing the chemical signatures of the first generations of stars (Bovill & Ricotti 2009; Frebel & Bromm 2012; Vargas et al. 2013; Frebel et al. 2014). The majority of UFDs contain only ancient stars, with the spread of ages being <2 Gyr (Muñoz et al. 2010; Brown et al. 2012; Vargas et al. 2013). Brown et al. (2012) found that the stellar populations of five UFDs: Hercules, Leo IV, Ursa Major I, Bootes 1 and Coma Berenices showed similar ages, suggesting that a global event such as reionization truncated their star formation. Weisz et al. (2014b) found that most galaxies with $M_* < 10^5\,M_\odot$ formed $\gtrsim$80% of their stars before $z \sim 2$, although there was significant variation between individual galaxies. For example, Canes Venatici II formed stars until ~8–11 Gyr ago, while Hercules and Leo IV formed 90 % of their stellar mass by 11–12 Gyr. The star formation history of UFDs indicates that at least some of them were forming stars at $z \sim 3$ and therefore must have contained neutral gas at this time. This suggests the possibility that very metal-poor DLAs trace gas in UFDs at the time they were forming stars.

With current instruments, it is difficult to observe UFDs beyond the local Milky Way + M31 system, although there has been one detection in the Virgo cluster (Jang & Lee 2014). The relationship between low-mass fossil galaxies that formed in the early universe and the observed UFDs today is therefore complicated by the influence of environment. Current observations cannot distinguish between systems which are true fossils of reionization and those that had their star formation quenched by other processes, such as tidal stripping (Weisz et al. 2014a). The UFDs that may be traced by DLAs need not be close to a host galaxy and could provide an opportunity to study the smallest galaxies in a less complicated environment.

Weisz et al. (2014b) studied 13 galaxies identified by Bovill & Ricotti (2011) as fossil candidates, finding that Hercules and Leo IV were the only strong candidates based on their star formation history. The Cooke DLAs trace gas at $z \sim 2$–4, indicating that the systems they trace were not permanently quenched by reionization. This is consistent with the Weisz

et al. (2014b) star formation histories for systems such as Canes Venatici II, for which the best fit model formed the bulk of its stars at $z \sim 2$. The mass of Canes Venatici II is $1.4 \times 10^6\,M_\odot$ within the half-light radius (Wolf et al. 2010), suggesting that even very low-mass systems can form stars at the redshifts of the Cooke DLAs.

In this work we use the hydrodynamical simulations of a $M_{\rm vir} = 10^7\,M_\odot$ galaxy from Bland-Hawthorn et al. (2015), in conjunction with the chemical evolution model from Webster et al. (2014), to investigate possible scenarios for the history and evolution of DLAs. Two main processes prevent galaxies with lower masses from forming or surviving in the early universe. The first is the energy output of massive stars. In previous work (Bland-Hawthorn et al. 2011, 2015; Webster et al. 2014), we presented hydrodynamical simulations of galaxies with formation masses of $10^7\,M_\odot$ and lower, showing that the limit for stars to retain gas and form stars in the face of feedback from their own star formation is $M_{\rm vir} \approx 10^{6.5}$–$10^7\,M_\odot$. Furthermore, our models were able to reproduce most features of the observed relationship between [α/Fe] and [Fe/H] in UFD galaxies.

The second process that can remove neutral gas from galaxies is the epoch of reionization, when the radiation from the first stars photoionized much of the neutral gas in the universe. It is often claimed (Rees 1986; Barkana & Loeb 1999; Gnedin 2000; Okamoto et al. 2008) that neutral gas is unable to cool onto halos with masses $\lesssim 10^8\,M_\odot$. However, more recent simulations (Bovill & Ricotti 2009) suggest that this is not a hard limit, with the influence of environment meaning that at least some lower-mass systems can survive the epoch of reionization. Ricotti & Gnedin (2005) used cosmological simulations to predict the existence of an undetected population of ultrafaint galaxies, around the same time as the first UFDs were observed.

We now consider whether $10^7\,M_\odot$ halos can explain the number of observed very metal-poor DLAs. For each $10^{11}\,M_\odot$ halo, there are $\sim 10^4$ halos with $M \leqslant 10^7\,M_\odot$. At $z \sim 2$–4, the virial radius of a $10^{11}\,M_\odot$ halo was $\sim$120 kpc (calculated from Bryan & Norman 1998), while the virial radius of a $10^7\,M_\odot$ halo was $\sim$0.5 kpc (see Figure 1 and Bland-Hawthorn et al. 2015). The ratio of cross-sectional area is proportional to the ratio of their radii squared, which is $\sim 2 \times 10^{-5}$. However, $10^7\,M_\odot$ halos are 10^4 times more common, so the total cross-sectional area is $\sim$20% that of the $10^{11}\,M_\odot$ halo. While this is only an approximate order of magnitude argument, it suggests that DLAs from $10^7\,M_\odot$ halos should be frequent enough to be observed.

In Section 2, we will summarize the simulations, although we refer to our previous work for the details. Section 3 compares the Cooke DLAs to our models. Possible scenarios for the history of the DLAs and their link to present-day UFDs are discussed in Section 4, followed by our conclusions in Section 5.

2. SIMULATIONS

The simulations used in this work are described in detail in Bland-Hawthorn et al. (2015) and Webster et al. (2014). In Bland-Hawthorn et al. (2015), we presented high-resolution simulations performed using the hydro/ionization code *Fyris Alpha* showing the effect of a $25\,M_\odot$ star on low-mass dark matter halos. An ionized region is created around the star prior to the supernova, resulting in the supernova having a much greater effect than for a lower-mass star. The thermal and ionization structures were calculated with the MAPPINGS IV ionization code, with the ATLAS9 atmospheric grid (Castelli & Kurucz 2004) and the Meynet & Maeder (2002) evolutionary tracks used to model the progenitor star. The full details can be found in Section 2 of Webster et al. (2014).

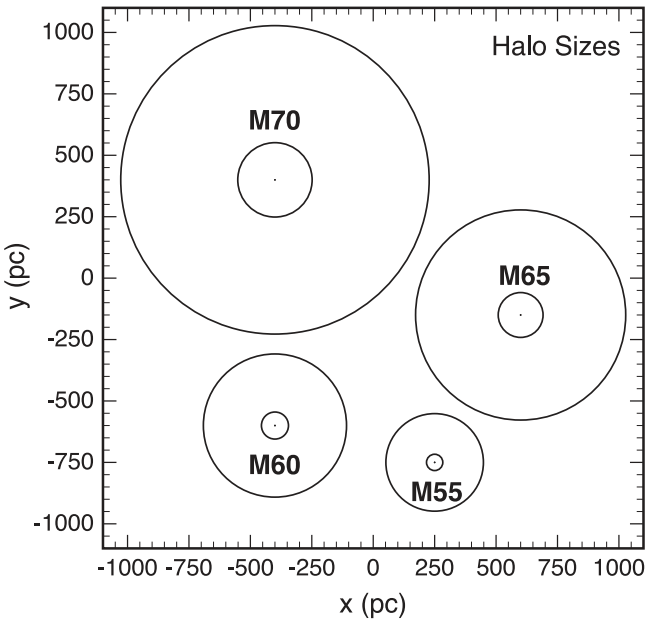

Figure 1. The physical sizes of the modeled halos at $z = 10$. M55 denotes a dark matter virial mass of $10^{5.5}\,M_\odot$, M60 has $M_{\rm vir} = 10^6\,M_\odot$ etc. The inner circles represent the scale radii, while the outer circles are the virial radii. For the off-centered explosion, the supernova is placed at the radius enclosing half the gas inside the scale radius, which is approximately halfway between the center and the scale radius. See Bland-Hawthorn et al. (2015) for the full set of parameters.

As a check for convergence, we investigated the amount of energy lost given a single-level resolution model, a two-level model with three times more cells in the central region, and a three-level model with the resolution again higher by a factor of three. If the resolution is insufficient, the gas has a tendency to overcool. The three models showed only minor differences, and we therefore used the two-level model with the higher resolution level of 216^3 cells having a resolution of $\sim$2 pc cell^{-1}. The other possible effect of insufficient resolution is that the metals will mix too efficiently.

The inclusion of radiative cooling and an inhomogeneous interstellar medium reduces the coupling between the supernova energy and the gas, such that halos with masses $M_{\rm vir} = 10^{6.5-7}\,M_\odot$ retain a large proportion of their baryons in the face of the ionization and supernova of the $25\,M_\odot$ star. The location of the star in the halo is also important, with supernovae occurring away from the center resulting in lower levels of enrichment and greater retention of dense gas.

The simulations start with an intergalactic medium (IGM) enriched to [Fe/H] = –4 by the first stars. Such low [Fe/H] has been observed in the IGM at $z \sim 3$–3.5 (Fumagalli et al. 2011). Our enhanced C, O and α elements ($[\alpha/{\rm Fe}]_{\rm init} = 0.7$) give $Z_{\rm init} = 10^{-3.2}\,Z_\odot$. We take our initial metallicity to be the critical threshold for low-mass star formation, such that low-mass star formation proceeds only after the initial $25\,M_\odot$ star enriches the

gas. While our threshold fits the critical metallicity $Z_{\rm crit} \sim 10^{-4}$–$10^{-3}\,Z_{\odot}$ of Smith & Sigurdsson (2007), other authors have suggested that this threshold could be as low at $Z_{\rm crit} \sim 10^{-6}\,Z_{\odot}$ (Schneider et al. 2006). As discussed in Webster et al. (2014), removing the assumption that low-mass stars do not form at our starting metallicity does not have a large impact on the results, as it affects only the first 10 Myr of the 600 Myr star formation history.

The gas mass within the scale radius r_s of the Einasto dark matter potential is set to be 10% of the dark matter mass within this radius. The overall baryon fractions $M_{\rm gas,vir}/M_{\rm vir}$ are ≈12%. The model of an $M_{\rm vir} = 10^7\,M_{\odot}$ halo contains 2.34 $\times\,10^5\,M_{\odot}$ of gas within r_s and 1.5 $\times 10^6\,M_{\odot}$ within $r_{\rm vir}$.

In the hydrodynamical simulations presented in Bland-Hawthorn et al. (2015), the evolution of the gas after a single supernova was traced for 60 Myr. Longer time periods were not possible in these high-resolution simulations due to the effect of boundary conditions, while difficulties involved with studying the interaction between supernovae restricted the models to a single supernova. In Webster et al. (2014), the density and metallicity of the gas after a single supernova was used as a template for the condition of the gas after subsequent supernovae. This allowed the density and metallicity of the gas to be tracked for 600 Myr. We model our halos in isolation, so do not include infall of diluting gas from the IGM, although we do consider the effects of dilution in Section 4.2, where the second burst of stars forms after the accretion of metal-poor gas.

The hydrodynamical simulation does not trace molecular cooling as would be required for the gas to cool to star formation temperatures. Instead, stars are allowed to form in the gas using the method of Argast et al. (2000), in which 10^4 cells are randomly selected, with each given a probability of forming a star proportional to the square of the density of the gas in the cell. The masses of the stars formed were selected by sampling a Kroupa (2001) initial mass function. After each supernova, the density distribution of the gas is reset to the distribution just after the supernova in the single-supernova hydrodynamical simulation and the density then evolves as for the hydrodynamical simulation. The metallicity is treated in the same way, except that it is added to rather than reset, such that the enrichment from each supernova adds to the enrichment from all previous supernovae.

The yields used to determine [Fe/H] and [α/Fe] are from Woosley & Weaver (1995), interpolated and extended to 8 $M_{\odot}$, taken to be the lowest mass star that ends its life as a supernova. After 100 Myr, SNe Ia occur with a probability equivalent to the SNe Ia rate determined by Jimenez et al. (2014), scaled to the star formation rates of our systems. The Type Ia yields are from Iwamoto et al. (1999).

Figure 1 shows the halos used in this work. The $M_{\rm vir} = 10^{5.5}\,M_{\odot}$, $10^6\,M_{\odot}$, $10^{6.5}\,M_{\odot}$ and $10^7\,M_{\odot}$ models are referred to as M55, M60, M65 and M70 respectively. The scale radius, which contains nearly all the gas sufficiently dense to be observed as DLAs, ranges from 33 pc for M55 to 151 pc for M70, while the virial radii range from 200 pc for M55 to 630 pc for M70. These halo properties are at $z = 10$. As shown in Figure 2, halos with $M_{\rm vir} = 10^{6-7}$ at $z = 10$ grow by an order of magnitude in both mass and radius by $z = 3$. Their virial radii grow from 0.3–0.6 to 1–3 kpc. The increase in halo mass will improve the gas retention compared to that of the first supernova. Our assumption that the first supernova occurs at $z = 10$ is supported by Power et al. (2014), which shows that halos with present-day masses $M_{\rm vir} < 10^9\,M_{\odot}$ reach the atomic cooling threshold at approximately this redshift.

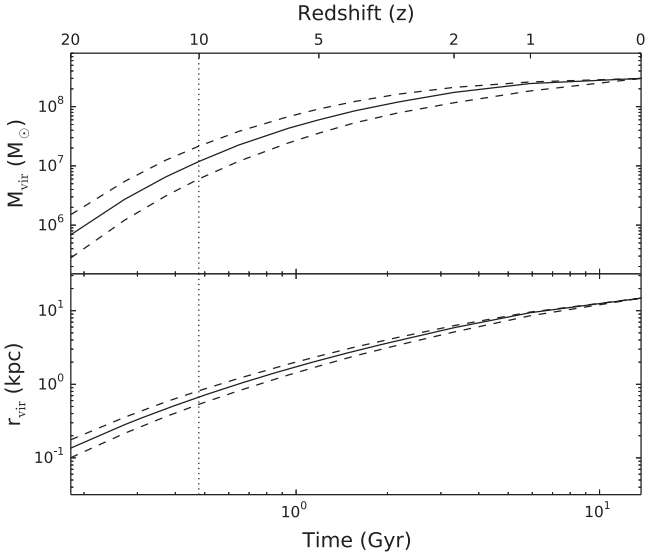

Figure 2. Evolution of the virial mass and radius for a halo with $M_{\rm vir} = 10^7\,M_{\odot}$ halo at $z = 10$ (indicated by the dotted line; see Figure 1) from $z = 20$ to the present time. This plot was produced using data from 5000 runs of the tree merger code of Parkinson et al. (2008). The dashed lines show the range which 67% of halos fall within.

The suffixes we use in the rest of this work represent the type of model: CCH represents a model with a central explosion, a clumpy ISM and a preionization phase, OCH is the same except with an off-centered explosion, while CCC and OCC represent models without a preionization phase. For example, the M65OCC model is a halo with $M_{\rm vir} = 10^{6.5}\,M_{\odot}$, which experiences an off-centered explosion (defined as a supernova at the radius enclosing half the gas mass within the scale radius) in a clumpy ISM, with no preionization phase. Only the Bland-Hawthorn et al. (2015) models with a clumpy ISM and radiative cooling are used, as these are the most realistic.

3. MODELED DLAS

In this section, we discuss the projected DLAs from the simulations discussed briefly in Section 2 and in detail in Bland-Hawthorn et al. (2015). The column densities and metallicities result from enrichment by a single supernova from [Fe/H] = −4. The metal-rich supernova ejecta were traced with a scalar variable, advected passively, such that the local enrichment of the gas could be determined at each time-step. Figures 3–5 show the distribution of column densities and metallicities along projected lines of sight, while Figures 6–9 show spatial maps of column density and metallicity. The state of the gas after 25 Myr is used, as this is sufficient time for the gas to recover from the supernova (Webster et al. 2014).

In this section, we assume that our halos exist in isolation and do not consider the complex possibility of mergers between low-mass gas-rich halos. A merger could introduce a fresh supply of low-metallicity gas, resulting in dilution as in the scenario considered in Section 4.2. This would result in higher column densities and lower metallicities, such that more sightlines would fit the DLA threshold. This would make it less likely that the systems could reach the metallicities of the DLAs with only a single supernova. The merger could also induce a burst of star formation. The effect of this is less

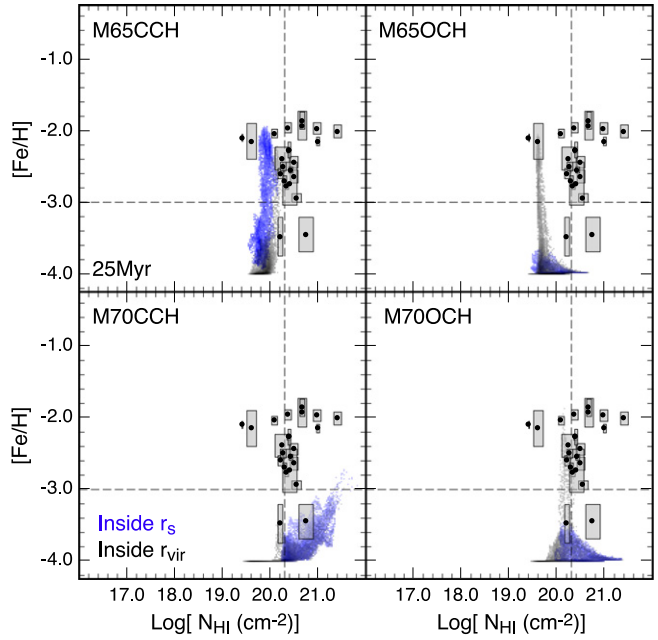

Figure 3. The distribution of H_I column density vs. projected metallicity 25 Myr after the explosion of a 25 $M_\odot$ star for the models with a preionization phase. The vertical dashed line indicates the definition of the minimum DLA column density. The Cooke et al. (2014) DLAs are also plotted with their error boxes.

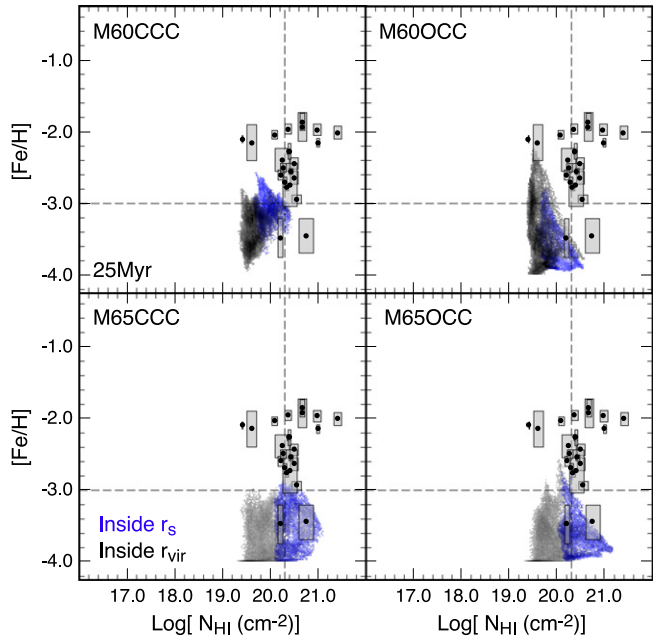

Figure 4. The distribution of H_I column density vs. projected metallicity 25 Myr after the explosion of a 25 $M_\odot$ star for the models without a preionization phase. The vertical dashed line indicates the definition of the minimum DLA column density. The Cooke et al. (2014) DLAs are also plotted with their error boxes.

certain, with possibilities including little or no change to the results, a more rapid increase in metallicity, or the removal of a large proportion of the gas in the system due to multiple supernovae close together in time.

We first discuss the models with a strong preionization phase from a 25 $M_\odot$ star, then the models with a weak preionization phase, consistent with an $M < 15\ M_\odot$ star.

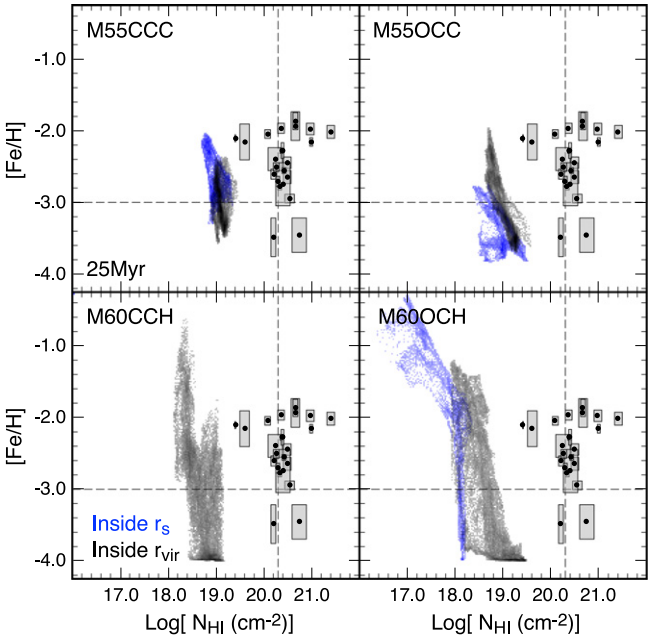

Figure 5. The distribution of H_I column density vs. projected metallicity 25 Myr after the explosion of a 25 $M_\odot$ star for M60 with a preionization phase and M55 without a preionization phase. The vertical dashed line indicates the definition of the minimum DLA column density. The Cooke et al. (2014) DLAs are also plotted with their error boxes.

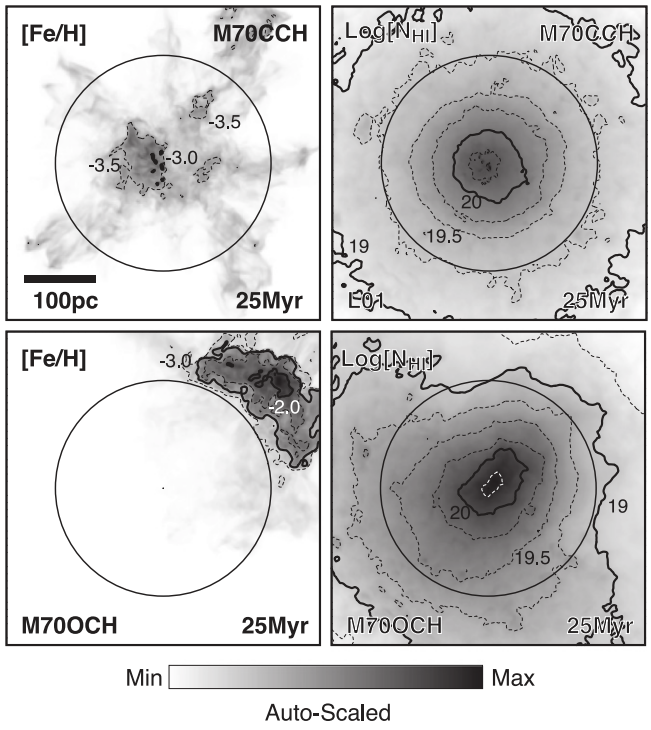

Figure 6. M70 model 25 Myr after the explosion of a 25 $M_\odot$ star. Top: central explosion. Bottom: off-centered explosion. The projected column densities are shown in the contour maps on the right, while the metallicities are shown on the left.

3.1. Strong Preionization Phase

As can be seen in the top panel of Figure 6, the M70CCH model retains a large amount of dense gas within the scale radius (150 pc), with the entire region having a column density

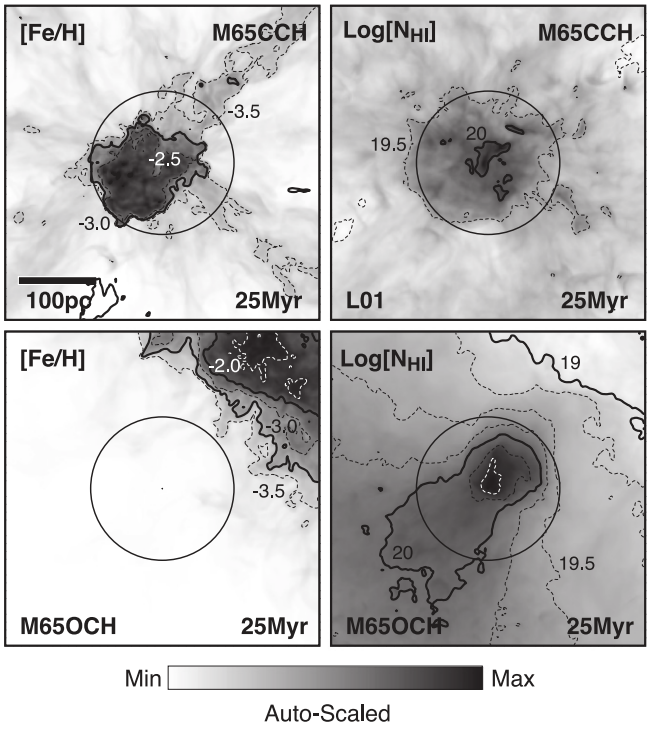

Figure 7. M65 model 25 Myr after the explosion of a 25 $M_{\odot}$ star. Top: central explosion. Bottom: off-centered explosion. The projected column densities are shown in the contour maps on the right, while the metallicities are shown on the left.

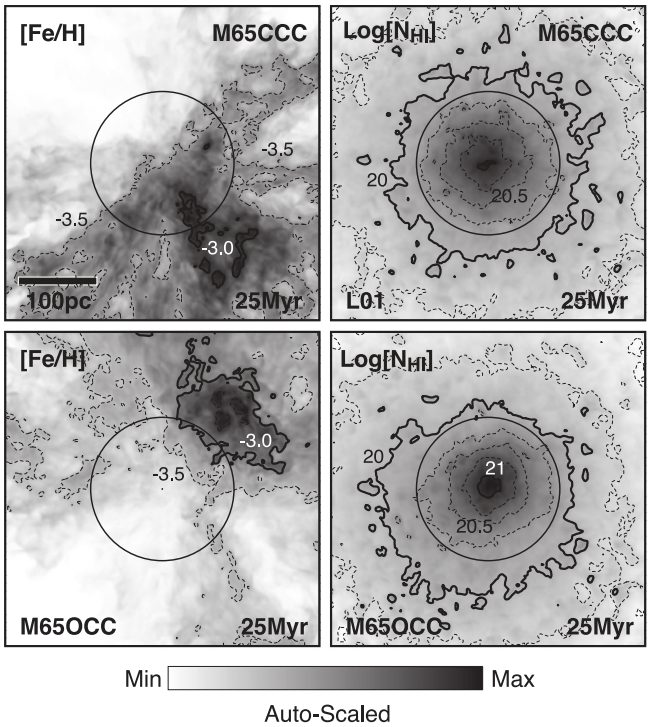

Figure 8. M65 model 25 Myr after the explosion of a star without a preionization phase. Top: central explosion. Bottom: off-centered explosion. The projected column densities are shown in the contour maps on the right, while the metallicities are shown on the left.

$N_{H_I} > 10^{19.25}\,\mathrm{cm}^{-2}$. A number of sightlines within 50 pc of the center are dense enough to be classified as DLAs. The metallicity of the densest region is [Fe/H] ∼ −3.5, with some

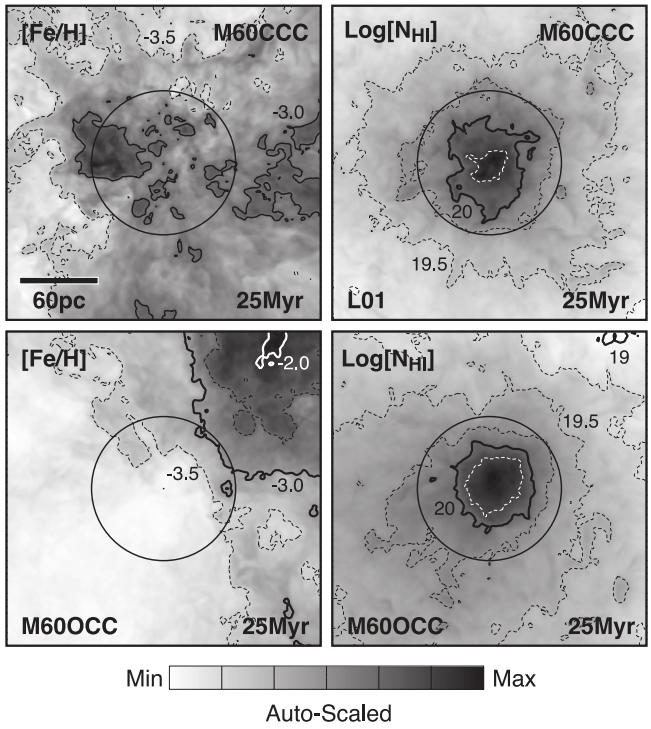

Figure 9. M65 model 25 Myr after the explosion of a star without a preionization phase. Top: central explosion. Bottom: off-centered explosion. The projected column densities are shown in the contour maps on the right, while the metallicities are shown on the left.

gas reaching [Fe/H] = −3.0. The bottom-left panel of Figure 3 shows that the highest density regions are the most metal-rich. This results from the central location of the supernova, such that the metals are initially deposited into the dense central region, along with it being the most massive model, such that more metals are retained close to the center rather than reaching the halo or escaping into the IGM. No other model shows this trend. Several sightlines in M70CCH reach column densities greater than $10^{21}\,\mathrm{cm}^{-2}$.

The M70OCH model is shown in the bottom panel of Figure 6. Unlike in the central case, the dense regions do not coincide with the higher metallicity regions. The metals from the off-centered explosion do not reach the central region and the densest gas is therefore not enriched. The bottom-right panel of Figure 3 show that there are a few sightlines outside the scale radius that reach [Fe/H] = −2.5 with column densities close to the minimum required to be defined as a DLA. These metallicities are higher than is seen in the central explosion model, but this is because there is less hydrogen gas in this region. The metal escape fraction is actually higher than in the central case because the metals can escape through the lower density regions away from the center. Most of the dense gas has [Fe/H] < −3.5 and the sightlines with column densities greater than $10^{-21}\,\mathrm{cm}^{-2}$ show almost no enrichment.

The M65CCH model shown in the top panel of Figure 7 has lower column densities than M70CCH with no sightline meeting the definition of a DLA. This model reaches higher [Fe/H] because there is less hydrogen. The total amount of metals is less than in the M70 case, as a greater proportion of the metals escape into the IGM as a result of the lower halo potential. The metallicity distribution in the top-left panel of Figure 3 does not show an increase in metallicity with

increasing column density because the enriched regions are those most affected by the supernova and therefore lose a significant amount of their dense gas.

The M65OCH model in the bottom panel of Figure 7 and the top-right panel of Figure 3 shows similar features to the M70OCH model, although the column densities are lower and the metallicities are higher for the same reasons as discussed for M65CCH. A few sightlines exceed the DLA threshold, however none of these are enriched above the starting metallicity [Fe/H] = −4. The lines of sight with the highest metallicity [Fe/H] ∼ −2 have column densities of $10^{19.6-19.8}$ cm^{-2}.

3.2. Weak Preionization Phase

The M65CCC model is shown in the top panel of Figure 8. The column density distribution is similar to M70CCH model, which is consistent with our finding in Bland-Hawthorn et al. (2015) that a decrease of 0.5 dex in halo mass has a similar effect on gas retention as switching off the preionization phase. [Fe/H] is higher than in the M70CCH model because the gas is less dense while the chemical yields from the star are the same. The metallicity distribution in the bottom-left panel of Figure 4 shows almost no variation with column density.

The M65OCC model in the bottom panel of Figure 8 also shows a similar column density distribution to its M70 counterpart with preionization, but once again the metallicity distribution is different. The lower gas densities in the M65 halo allow some metals to reach and enrich the dense gas in the center. This can be seen in the bottom-right panel of Figure 4, where some of the gas within the scale radius reaches [Fe/H] > −3.

The lack of a preionization phase means that even M60 halos can retain sufficient gas to reach the DLA threshold, as is shown in Figure 9. In M60CCC, a few sightlines reach column densities of $10^{20.3}$ cm^{-2} with [Fe/H] = −3.0. Unlike in the M65 case, there is no gas within the scale radius with [Fe/H] < −3.5, showing that the supernova has enriched all the central gas. As shown in the top-left panel of Figure 4, this is the only system other than M70CCH for which metallicity increases with column density.

The M60OCC model shows a low density, high metallicity region near the supernova which is a feature of all the models with an off-centered explosion. The top-right panel of Figure 4 shows that the regions with column densities exceeding the DLA threshold remain unenriched.

Figure 5 shows the lowest mass systems we modeled. The M60CH models and the M55CC models do not retain dense gas in the face of the supernova explosion, with the maximum column density being $10^{19-19.5}$ cm^{-2}. In the off-centered cases the densest gas remains unenriched, while the models with a central explosion retain gas with a column density of 10^{19} cm^{-2} with [Fe/H] ∼ −2.5.

3.3. Comparison with the Cooke DLAs

In this section we compare our models above to the 23 observed very metal-poor DLAs presented by Cooke et al. (2014). These DLAs have redshifts of $z = 2.1-4.5$, [Fe/H] ranging from −3.48 to −1.86, and column densities $\log(N_{H_I}/cm^{-2}) = 19.6$–21.4. Figures 3–5 show that most of the DLAs have metallicities higher than for our modeled DLAs, with the highest metallicities in our models resulting from low amounts of neutral hydrogen and therefore low column densities. This suggests that enrichment from a single supernova is generally not sufficient to explain the observed DLAs. We will discuss extended star formation in Section 4. However, a few DLAs could be explained by enrichment from a single star.

Table 1
Properties of DLAs Compared to Our Model

Property	M70	M65	⟨DLAs⟩	$DLAs_{max}$	$DLAs_{min}$
T_{gas} (K)	4860	2300	9600	17,000	5600
$\log(n(H)/cm^{-3})$	−0.13	−0.07	−1.0	−0.35	−1.3
r_{H_I} (pc)	150	91	220	1270	32
M_{WNM} (10^5 $M_\odot$)	2.3	0.7	2.5	220	⩽0.4
c_s	5.8	4.0	8.0	10.7	6.1

Note. The masses, radii and densities for the models are taken at the scale radius of the Einasto potential.

Two systems show [Fe/H] ∼ −3.5. The gas masses are not known for these systems, although one has an upper limit of $M_{WNM} < 6.3 \times 10^6$ $M_\odot$. In our M70CH models, which have a gas mass of 10^6 $M_\odot$ within r_{vir} and 2×10^5 $M_\odot$ within r_s, the 25 $M_\odot$ star enriches the surrounding gas to metallicities ranging from [Fe/H] = −4.0 to −3.0. The two lowest metallicity DLAs are therefore consistent with enrichment by a single supernova in a 10^7 $M_\odot$ halo. The M65CCC model also shows sightlines with the correct column density and metallicity. These two DLAs may therefore trace gas polluted only by a single supernova. This level of [Fe/H] is consistent with that suggested by Bromm & Yoshida (2011) for the first galaxies, so they may even only be enriched by Population III stars.

Two other DLAs could be explained by enrichment from a single supernova if they are lower-mass systems. HS0105+1619 and J2155+1358 have column densities ≈$10^{19.5}$ cm^{-2} and [Fe/H] ≈ −2.1. This is consistent with the M65CH models. However, both show [α/Fe] <0.3, which is difficult to explain given enrichment from a 25 $M_\odot$ star. The chemical abundances are more consistent with the higher column density systems, so it is more likely that they have experienced an extended period of star formation followed by losing most of their gas. The column densities are consistent with the systems that form no further stars in our models.

The remainder of the DLAs have metallicities too high to be explained by a single supernova. However, in Webster et al. (2014) we showed that the gas recovers from the impact of a 25 $M_\odot$ star in less than 25 Myr for an M70 halo regardless of supernova location. Furthermore, the M65 models without a preionization phase show little evidence of disruption or gas loss, suggesting that stars less massive than 25 $M_\odot$ are unlikely to blow out a significant proportion of the gas in an M70 system. Our DLA models are therefore likely to remain relevant for subsequent supernovae.

Cooke et al. (2014) determined the thermal contribution to the line broadening for 12 clouds in 9 of the 23 systems, allowing gas properties to be calculated. The total warm neutral medium gas masses range from less than 3×10^4 to 2×10^7 $M_\odot$. A comparison between the properties of the gas in our model and the properties determined for these DLAs is shown in Table 1. The neutral hydrogen density $n(H)$, the cloud radius r_{H_I} and the warm neutral gas mass M_{WNM} for our model are at the scale radius. It is possible that the gas observed

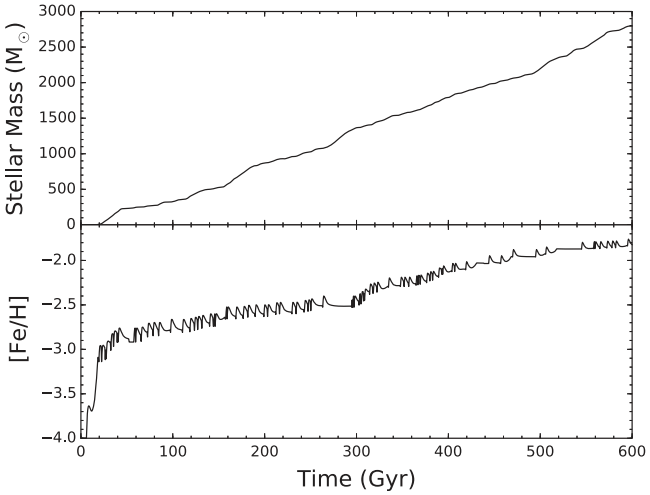

Figure 10. The gas and metallicity evolution as a function of time for one realization of the single-burst scenario in our simulations. Top: the total star formation since $t = 0$. Bottom: the mean metallicity of the gas within the $(200\,\mathrm{pc})^3$ main simulation level as a function of time.

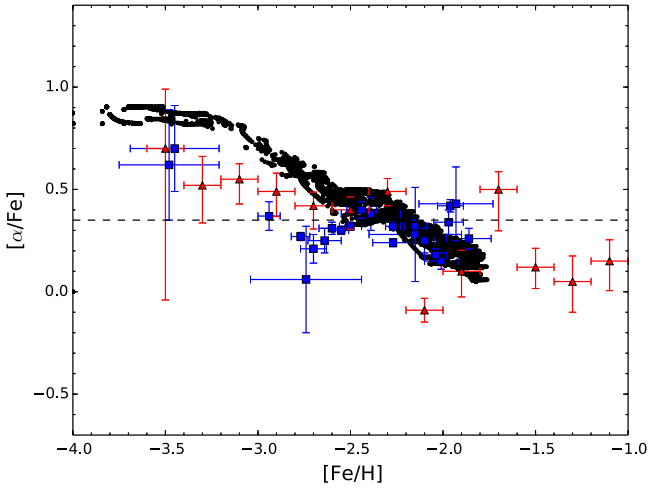

Figure 11. [α/Fe] vs. [Fe/H] for our simulation for five simulation runs (black points), the Vargas et al. (2013) sample of stars in UFDs in 0.2 dex metallicity bins (red triangles), and the Cooke et al. (2014) DLAs (blue squares).

in DLAs extends beyond these radii, which would result in lower densities and higher gas masses. The temperature and sound speed are slightly lower in the models than for the observations. Overall, the DLAs for which these physical quantities could be determined are consistent with halos with $10^7\,M_\odot$ or slightly higher.

4. ENRICHMENT OF THE DLAS

In this section we will discuss two possible enrichment histories for the DLAs that show evidence of extended star formation. The first scenario suggests that they have been enriched only by a single burst of stars, with the alternative being that they are a mix of systems which have been enriched by one burst and those which have been enriched by two bursts following the accretion of metal-poor gas. As discussed in Webster et al. (2014) and Bland-Hawthorn et al. (2015), only the M70CH and the M65CC models retain dense enough gas for extended low mass star formation. This section focuses on the M70CH model, using the chemical evolution model of Webster et al. (2014).

4.1. Single Burst

The single-burst scenario explains the relationship between [α/Fe] and [Fe/H] in the following way:

1. Gas enriched to [Fe/H] ~ -4 condenses onto a dark matter halo.
2. Low-mass star formation commences and Type II supernovae (SNe II) enriches the gas, resulting in an increase in [Fe/H] and a decrease in [α/Fe]. [α/Fe] declines at low [Fe/H] due to SNe II from lower-mass (8–15 $M_\odot$) stars, which have a mean [α/Fe] of 0.2 (Woosley & Weaver 1995; Nomoto et al. 2006, extrapolated to 8 $M_\odot$). This decline commences at lower [Fe/H] than in our model.
3. After $t \sim 100$ Myr, SNe Ia enrich the gas, resulting in a decline in [α/Fe] with increasing [Fe/H]. This decline is observed in DLAs with [Fe/H] > -2.0 (Vladilo et al. 2011).

The stellar mass and gas metallicity evolution in one simulation run for this scenario is shown in Figure 10. Our model is stochastic, such that different simulation runs will provide different results, but the overall features are similar. The star formation rate is on average constant with time, but is bursty, with several short periods of little or no star formation following each supernova explosion. Each supernova causes a large jump in the mean metallicity in the central region, which is caused by the deposition of new metals onto the grid, along with the lower metallicity gas being pushed outwards beyond the inner $(200\,\mathrm{pc})^3$ region considered here. The mean metallicity in this region then decreases as gas returns to the center, although some of the metals have mixed with the gas and the overall metallicity therefore remains higher than before the supernova.

Figure 11 shows [α/Fe] versus [Fe/H] for the Cooke et al. (2014) DLA observations compared to the gas in our simulation, as well as observations of stars in UFDs from Vargas et al. (2013). The three are reasonably consistent for [Fe/H] $\gtrsim -2.5$. However, at lower metallicities both our model and the UFD observations show a gradual decline in [α/Fe] with [Fe/H], while the DLAs show a rapid decline between [Fe/H] ~ -3.5 and -2.8, with [α/Fe] then remaining constant until [Fe/H] $= -2.0$. The mean [α/Fe] abundance of 0.25 for the DLAs for $-3 <$ [Fe/H] < -2.5 is also lower than the average of 0.35 for SNe II in a Kroupa or Salpeter IMF, which is observed in stars in the halo of the Milky Way (Frebel & Bromm 2012).

Cooke et al. (2014) also notes the suppression in [α/Fe] for the DLAs compared to stars in the overall population of dSph galaxies. They suggest that this could be caused by small number statistics, modeling techniques, or physical differences between the two populations. Karlsson et al. (2012) suggested two classes of explanations for suppressed [α/Fe] in a star cluster in Sextans. The first explains the low [α/Fe] by contribution from SNe Ia at low [Fe/H]. This could result either from the accretion of low metallicity gas, reducing [Fe/H] at a time when SNe Ia contribute to the enrichment, or from a very low star formation rate. The second class of explanations involve only SNe II. Aoki et al. (2009) note that a truncated IMF at high masses would result in lower [α/Fe], because higher mass stars yield more alpha elements. Weidner &

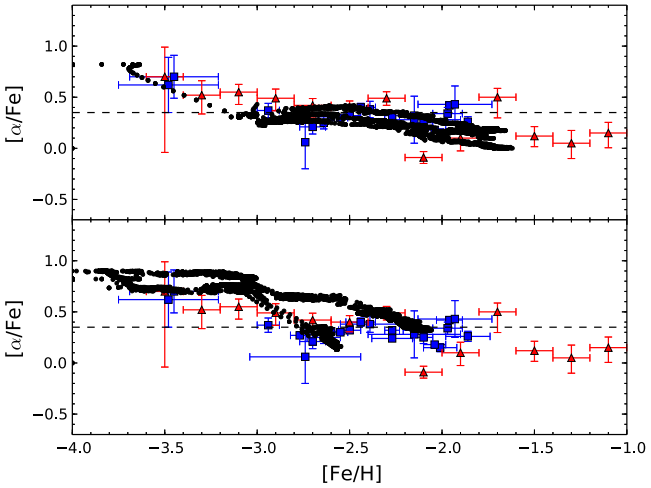

Figure 12. Top: single burst scenario with truncated IMF at the high mass end. Bottom: two burst scenario with accretion of low [Fe/H] gas after the first burst. [α/Fe] vs. [Fe/H] for three simulation runs in each plot is represented by black points, the Vargas et al. (2013) sample of stars in UFDs in 0.2 dex metallicity bins by red triangles, and the Cooke et al. (2014) DLAs by blue squares.

Kroupa (2005) suggest that such an IMF is required for systems with very low star formation, which are likely to have low cluster masses, limiting the maximum mass for a star that can form in the cluster. The final alternative discussed is hypernovae, which produce more Fe than normal SNe II. However, based on iron-peak element abundances, Cooke et al. (2013) suggest that very metal-poor DLAs were enriched by stars that exploded as core collapse supernovae which released 1.2×10^{51} erg of energy.

The question of whether SNe Ia are responsible for the suppression of [α/Fe] in DLAs is not easily resolved. However, assuming the DLAs are first-burst systems and a reasonably homogeneous population, explanations for the decline in [α/Fe] between [Fe/H] = −3.5 and −2.5 involving SNe Ia are unable explain the constant [α/Fe] for −2.5 < [Fe/H] < −2.0. It is more likely that for a single burst, SNe Ia start occurring at [Fe/H] ≈ −2.0 as was concluded by Cooke et al. (2014).

Given that enrichment by SNe Ia is unlikely to explain the low [α/Fe] for −2.5 < [Fe/H] < 2.0, the single-burst scenario requires that supernovae with lower mass yields have enriched the gas observed in DLAs. One possibility for this is that DLAs are enriched by low-mass (8−15 $M_\odot$) SNe II to a level lower than the average [α/Fe] for a Kroupa or Salpeter IMF. One possible explanation for this is that for the reasons discussed above, the IMF is truncated at the high mass end. We model an IMF truncated at 20 $M_\odot$, with the results shown in the top panel of Figure 12. [α/Fe] remains slightly enhanced compared to the [Fe/H] ∼ −2.5 DLAs. Reducing the highest mass further would fit the lowest metallicity DLAs, but could not simultaneously explain the DLAs with [Fe/H] > −2.5.

Another possible explanation is a selection effect. In Bland-Hawthorn et al. (2015) we studied the effect of a 25 $M_\odot$ star on halos with masses 10^6−10^7 $M_\odot$. It was found that a strong preionization phase evacuates the region close to the star, resulting in the subsequent supernova having a much larger effect on the ISM than it would in the case of a <15 $M_\odot$ star with a much weaker preionization phase. In particular, a 25 $M_\odot$ star in a $10^{6.5}$ $M_\odot$ halo can terminate star formation (Webster et al. 2014). It is therefore possible that systems which have experienced lower-mass stars and therefore lower [α/Fe] are more likely to contain dense gas and be observed as DLAs. This would have a similar effect to the truncated IMF as in the top panel of Figure 12.

The above explanations provide a number of possible ways that SNe II could result in the suppressed [α/Fe] seen in very metal-poor DLAs compared to the Kroupa IMF. However, it does not explain why the DLAs show lower [α/Fe] compared to stars in UFDs, showing [α/Fe] lower by 0.25 dex for −3.0 < [Fe/H] < −2.5. None of the observed UFDs has mean [α/Fe] < 0.4 for [Fe/H] < −2.5. We therefore conclude that if all DLAs are systems forming their first burst of stars, either they are not representative of the UFD population, or there are systematic differences that arise in the process of measuring [α/Fe] between gas in DLAs and stars in UFDs. It is possible that as a result of evolution, the DLAs are not representative of UFDs as observed today. Many of the DLAs contain sufficiently dense gas to continue forming stars. In the next section we consider a scenario where the difference between the two classes of systems is explained by the DLAs being observed at different points in their evolution.

4.2. Two Bursts

We now investigate a scenario in which the DLAs are a mix of systems that have formed only one burst of stars, and systems that have formed or are forming their second burst of stars after the accretion of metal-poor gas. Weisz et al. (2014b) investigated the star formation history of 38 Local Group dwarf galaxies, including four of the UFDs studied in Vargas et al. (2013). They found that Hercules was consistent with having formed all its stars in one burst before and during reionization. Leo IV also shows only one burst, but likely formed stars until $z \sim 2$. Leo T and Canes Venatici II have a more extended star formation history, although Leo T shows no star formation from $z = 1$–5. The best fit model to Canes Venatici II shows a burst of star formation commencing at $z \sim 2.5$, while the 1σ uncertainty is consistent with 80% of the stars being formed in a single burst ending at $z \sim 2.5$. This suggests that star formation occurred in some UFDs at the redshifts of the Cooke et al. (2014) DLAs, and that some were forming their first burst of stars, while others were forming their second burst.

We now compare the DLA population to the stars in Leo IV and Canes Venatici II, the two systems which are likely to form stars at the redshifts of the Cooke et al. (2014) DLAs. The results are shown in the bottom panel of Figure 12. The four stars in Leo IV are consistent with the [α/Fe] abundances of the DLAs, while of the six stars in Canes Venatici II with [Fe/H] < −1.5, 4 show [α/Fe] enhanced significantly above that of the DLAs. It should be noted that while Weisz et al. (2014b) find that the best fit for the star-forming history of Canes Venatici II is a model with multiple bursts, Brown et al. (2014) argue for a single burst. We present the following possible scenario for its evolution. The stars with [α/Fe] ∼ 0.8 formed in the first burst, followed by reionization or supernova feedback turning star formation off. The galaxy accreted low-metallicity gas which was then polluted by SNe Ia. The second burst of stars therefore formed at a lower [α/Fe] for a given [Fe/H].

If the DLAs trace gas in UFDs, it is likely that we are observing some of them during or before their second burst of star formation. This provides an explanation as to why the DLAs tend to have lower [α/Fe] at low [Fe/H] when compared to the UFDs and the average expected from SNe II. High [α/Fe]

stars formed in the first burst of star formation before and during reionization, followed by a pause in star formation. By the time of the second burst of star formation, sufficient time has passed for SNe Ia to occur, resulting in the reduced [α/Fe] seen in the DLAs. This also provides an explanation for low [α/Fe], low [Fe/H] stars in systems such as Canes Venatici II and Ursa Major I.

In the two-burst model, the DLAs in the clump at [Fe/H] ~ -2.0 in Figure 12 are forming their first burst of stars, while those in the clump at [Fe/H] ~ -2.5 are forming their second burst. This scenario predicts the existence of [α/Fe] $= 0.5$–0.7 systems at [Fe/H] ~ -2.5, which have not yet been observed.

4.3. Other Possibilities

A third possibility is that the DLAs do not evolve from the clump at [Fe/H] ~ -2.5 to the clump at [Fe/H] ~ -2.0, but that they instead represent systems with different masses and star formation histories. Cooke et al. (2014) found that systems with higher velocity widths showed higher metallicities. While it is impossible to extrapolate directly to halo mass, systems with lower velocity widths will on average have lower halo masses. The [Fe/H] ~ -2.5 systems may therefore represent systems which correspond to UFDs, while the higher metallicity systems may be classical dwarf spheroidals. However, this does explain why the DLAs are observed with [α/Fe] ~ 0.3, when SNe Ia could suppress [α/Fe] below this level.

Our models in Section 4 showed that systems such as M65CH which do not show star formation can still reach the DLA column density limit along some sightlines. Some of the DLAs may therefore be systems that are not forming stars at the time they are observed. The clump at [Fe/H] ~ -2.5 could be systems which formed few stars, with most of the enrichment coming from later SNe Ia, while the [Fe/H] ~ -2.0 systems can be explained by the single-burst model. Observations of neutron-capture elements such as barium may be able to provide support for or rule out this scenario. Neutron-capture abundances could also test the possibility that the [α/Fe] abundances result from a bimodal SN Ia delay-time distribution (Mannucci et al. 2006; Yates et al. 2013), in which approximately 50% of the supernovae occur at $t \sim 50$ Myr. This could result in an early decline in [α/Fe], followed by a period of few SNe Ia, during which [α/Fe] is flat with [Fe/H], as is observed in the DLAs.

An alternative explanation for the variation in [α/Fe] is the enrichment of some DLAs by pair-instability supernovae. Pair-instability supernovae eject a large amount of iron, resulting in low [α/Fe]. Wise et al. (2012) suggest this as an explanation for the apparent metallicity floor of DLAs at [Fe/H] $= -3$. The only exceptions are two DLAs with high [α/Fe] show [Fe/H] < -3, which these may have been enriched by an event with more usual supernova yields. In future work we will investigate different types of supernovae, such as hypernovae and pair-instability supernovae, to determine their effect on our higher mass models.

Finally, we note that factors outside the scope of our model could affect our result. For example, in this work we assume that all metal species mix into the gas in the same way. While different elements may have different dust formation timescales, the gas and dust physics involved is difficult to track. The best work to date on this issue has involved considering the dust and molecular gas phases in post-processing (Krumholz & Gnedin 2011; Gnedin & Draine 2014). These complicated issues will be considered in future work. However, none of the scenarios in this subsection can resolve the discrepancy between the UFDs and the DLAs, requiring different enrichment histories for the two classes of systems

5. CONCLUSIONS

Using simulations of star formation and chemical enrichment in systems with dark matter halo masses of $10^7\,M_\odot$, we have modeled the chemical abundances of very metal-poor DLAs. Our conclusions follow:

1. For the DLAs in which Cooke et al. (2014) were able to derive physical quantities, the measured sound speeds, temperatures, gas masses and gas densities are mostly consistent with gas in our modeled $M_{\rm vir} = 10^7\,M_\odot$ halo, although the temperature and sound speed are slightly too low, suggesting the observed DLAs may have slightly larger halo masses.
2. The column densities of the Cooke et al. (2014) DLAs can be reproduced by models of gas in a $10^7\,M_\odot$ halo which include feedback from the preionization and supernova of a massive star.
3. Multiple supernovae are required to explain the metallicities of 21 of the 23 Cooke et al. (2014) DLAs, except in the case of a pair-instability supernova as in Wise et al. (2012).
4. Our model of star formation and chemical enrichment can reproduce [α/Fe] for DLAs with $-2.5 \lesssim$ [Fe/H] $\lesssim -2.0$. While there is significant scatter for individual systems, the average UFD abundances also agree.
5. For $-3.0 \lesssim$ [Fe/H] $\lesssim -2.5$ there is some tension between our model and the DLA abundances, with the DLAs showing mean [α/Fe] $= 0.25$, while our model has [α/Fe] ~ 0.5. [α/Fe] is also suppressed for the DLAs compared to the average stellar metallicity in UFDs and compared to the mean expected for SNe II for a Kroupa or Salpeter IMF.
6. One explanation for the abundances of DLAs is a scenario with a truncated IMF, or a selection effect where only systems with lower mass supernovae retain their gas and are therefore observed as DLAs. However, this does not explain the the suppression of [α/Fe] compared to abundances of stars in UFDs.
7. A scenario that can explain the mismatch between the DLA and UFD abundances assumes that the [Fe/H] $= -3.0$ to -2.5 DLAs have been enriched by two bursts, while the higher [Fe/H] DLAs have been enriched by only one. Two-burst DLAs form their first burst before reionization before losing all their neutral gas. At a later time, they accrete low-metallicity gas and commence a second burst of star formation. SNe Ia from first burst stars enrich the gas without a delay time. However, this scenario does not explain why no DLAs have been observed at [Fe/H] ~ -2.5 with high [α/Fe].
8. It is possible that the [Fe/H] $= -3.0$ to -2.5 and the [Fe/H] $= -2.5$ to -2.0 DLAs have very different star formation histories. For example, the low [Fe/H] systems may have formed few stars and therefore experienced few or no SNe II. These systems were then enriched at a later time by one or more SNe Ia, resulting in the low observed

[α/Fe]. The higher [Fe/H] systems would then be explained by the single-burst scenario.

We thank the anonymous referee for useful comments which greatly improved the clarity and quality of this work. DW is funded by an Australian Postgraduate Award.

REFERENCES

Aoki, W., Arimoto, N., Sadakane, K., et al. 2009, A&A, 502, 569
Argast, D., Samland, M., Gerhard, O. E., & Thielemann, F.-K. 2000, A&A, 356, 873
Barkana, R., & Loeb, A. 1999, ApJ, 523, 54
Bird, S., Vogelsberger, M., Sijacki, D., et al. 2013, MNRAS, 429, 3341
Bland-Hawthorn, J., Sutherland, R., & Karlsson, T. 2011, in EAS Publications Ser 48, in A Universe of Dwarf Galaxies, ed. M. Koleva, P. Prugniel, & I. Vauglin (Cambridge: Cambridge Univ. Press), 397
Bland-Hawthorn, J., Sutherland, R., & Webster, D. 2015, ApJ, in press
Bovill, M. S., & Ricotti, M. 2009, ApJ, 693, 1859
Bovill, M. S., & Ricotti, M. 2011, ApJ, 741, 18
Bromm, V., & Yoshida, N. 2011, ARA&A, 49, 373
Brown, T. M., Tumlinson, J., Geha, M., et al. 2012, ApJL, 753, L21
Brown, T. M., Tumlinson, J., Geha, M., et al. 2014, ApJ, 796, 91
Bryan, G. L., & Norman, M. L. 1998, ApJ, 495, 80
Castelli, F., & Kurucz, R. L. 2004, arXiv:0405087
Cen, R. 2012, ApJ, 748, 121
Cooke, R., Pettini, M., & Jorgenson, R. A. 2014, arXiv:1406.7003
Cooke, R., Pettini, M., Jorgenson, R. A., et al. 2013, MNRAS, 431, 1625
Cooke, R., Pettini, M., Steidel, C. C., Rudie, G. C., & Jorgenson, R. A. 2011a, MNRAS, 412, 1047
Cooke, R., Pettini, M., Steidel, C. C., Rudie, G. C., & Nissen, P. E. 2011b, MNRAS, 417, 1534
Frebel, A., & Bromm, V. 2012, ApJ, 759, 115
Frebel, A., Simon, J. D., & Kirby, E. N. 2014, ApJ, 786, 74
Fumagalli, M., Prochaska, J. X., Kasen, D., et al. 2011, MNRAS, 418, 1796
Gnedin, N. Y. 2000, ApJ, 542, 535
Gnedin, N. Y., & Draine, B. T. 2014, ApJ, 795, 37
Iwamoto, K., Brachwitz, F., Nomoto, K., et al. 1999, ApJS, 125, 439
Jang, I. S., & Lee, M. G. 2014, ApJL, 795, L6
Jimenez, N., Tissera, P. B., & Matteucci, F. 2014, arXiv:1402.4137
Jorgenson, R. A., & Wolfe, A. M. 2014, ApJ, 785, 16
Karlsson, T., Bland-Hawthorn, J., Freeman, K. C., & Silk, J. 2012, ApJ, 759, 111
Krogager, J.-K., Fynbo, J. P. U., Møller, P., et al. 2012, MNRAS, 424, L1
Kroupa, P. 2001, MNRAS, 322, 231
Krumholz, M. R., & Gnedin, N. Y. 2011, ApJ, 729, 36
Mannucci, F., della Valle, M., & Panagia, N. 2006, MNRAS, 370, 773
Meynet, G., & Maeder, A. 2002, A&A, 390, 561
Muñoz, R. R., Geha, M., & Willman, B. 2010, AJ, 140, 138
Nomoto, K., Tominaga, N., Umeda, H., Kobayashi, C., & Maeda, K. 2006, NuPhA, 777, 424
Okamoto, T., Gao, L., & Theuns, T. 2008, MNRAS, 390, 920
Parkinson, H., Cole, S., & Helly, J. 2008, MNRAS, 383, 557
Pontzen, A., Governato, F., Pettini, M., et al. 2008, MNRAS, 390, 1349
Power, C., Wynn, G. A., Robotham, A. S. G., Lewis, G. F., & Wilkinson, M. I. 2014, arXiv:1406.7097
Rees, M. J. 1986, MNRAS, 218, 25P
Ricotti, M., & Gnedin, N. Y. 2005, ApJ, 629, 259
Schneider, R., Omukai, K., Inoue, A. K., & Ferrara, A. 2006, MNRAS, 369, 1437
Smith, B. D., & Sigurdsson, S. 2007, ApJL, 661, L5
Tinsley, B. M. 1979, ApJ, 229, 1046
Vargas, L. C., Geha, M., Kirby, E. N., & Simon, J. D. 2013, ApJ, 767, 134
Vladilo, G., Abate, C., Yin, J., Cescutti, G., & Matteucci, F. 2011, A&A, 530, A33
Webster, D., Sutherland, R., & Bland-Hawthorn, J. 2014, ApJ, 796, 11
Weidner, C., & Kroupa, P. 2005, ApJ, 625, 754
Weisz, D. R., Dolphin, A. E., Skillman, E. D., et al. 2014a, ApJ, 789, 147
Weisz, D. R., Dolphin, A. E., Skillman, E. D., et al. 2014b, ApJ, 789, 148
Wise, J. H., Turk, M. J., Norman, M. L., & Abel, T. 2012, ApJ, 745, 50
Wolf, J., Martinez, G. D., Bullock, J. S., et al. 2010, MNRAS, 406, 1220
Woosley, S. E., & Weaver, T. A. 1995, ApJS, 101, 181
Yates, R. M., Henriques, B., Thomas, P. A., et al. 2013, MNRAS, 435, 3500